

Room-temperature low-cycle fatigue and fracture behaviour of asymmetrically rolled high-strength 7050 aluminium alloy plates

L. G. Hou^{1,2*}, W. L. Xiao¹, H. Su¹, C. M. Wu³, D. G. Eskin^{2*}, L. Katgerman⁴, L. Z. Zhuang¹, J. S. Zhang¹

¹ State Key Laboratory for Advanced Metal and Materials, University of Science and Technology Beijing, No.30 Xueyuan Road, Haidian District, Beijing 100083, China

² BCAST, Brunel University London, Uxbridge, Middlesex, UB8 3PH, UK

³ Nanjing Qizhi Pujiao Transportation Technology, Co., Ltd, No.8 Lanhua Road, Pukou District, Nanjing, 211800, China

⁴ Katgerman Aluminium Technology, van Beuningenlaan 10, 2334CC Leiden, Netherlands

Corresponding author. *E-mail address*: lghou@skl.ustb.edu.cn (L. G. Hou), Dmitry.Eskin@brunel.ac.uk (D. G. Eskin).

Abstract: The asymmetrical rolling (ASR) process with shear deformation is considered as a promising technology to adjust/improve through-thickness microstructure homogeneity and integrated properties of high-strength aluminium alloy plates. But the advantages may come with caveats that are the subject of our research. In this paper, the room-temperature low cycle fatigue properties and fracture behaviour of the ASR-ed AA7050 aluminium alloy plates are compared with the symmetrical rolling (SR) one. It is shown that after either type of rolling the plates exhibit similar low-cycle fatigue lives but the SR-ed one displays a better cyclic deformation ability and slightly higher fatigue lives at high strain amplitudes. It is demonstrated that the severe surface-localized deformation induced by ASR and SR processes contributes to the formation of slip relief on the surface and subsequently initiate micro-cracks that are propagated via transgranular and/or intergranular modes along with obvious fatigue striations. Recrystallised grains with coarse grain boundary precipitates and wide precipitate-free zones near the upper/bottom layers as well as more numerous and larger secondary particles in the ASR-ed plates may cause early crack initiation for a short crack initiation life. However, the SR-ed plate with more frequent subgrains near surface layers, numerous fine subgrains and less indissoluble particles could possess better crack initiation/propagation resistance and cyclic loading behaviour. Fine subgrains with higher microhardness/strength can facilitate passing of dislocations or slip bands into adjacent grains so as to delay crack propagation such as via

energy-intensified transgranular fracture for extending fatigue life. Properly balancing the through-thickness strain/deformation distribution and recrystallization/indissoluble particle formation via implementing a feasible ASR process becomes a critical issue in forming fracture-resistant microstructures for high-strength aluminium alloy plates. The underlying causes/mechanisms regarding the differences of microstructures and mechanical behaviour are revealed and discussed based on modelling through-thickness temperature/strain distributions and detailed microstructure characterization.

Key words: high-strength aluminium alloy; low-cycle fatigue; microstructure; fracture; precipitation

1. Introduction

Regarding critical structural materials for aerospace applications, the integrated properties of high-strength aluminium alloys, i.e., strength, toughness, corrosion resistance, fatigue life, are extensively determined by the intricate interaction of composition, microstructure and processing (i.e., heat treatment, rolling, forging, etc.), with the pivotal role of controlling and tuning grain structures, inter-/intra-granular precipitation, constitutive particles, etc.^[1-6]. For example, the strength, toughness and corrosion resistance are dictated by inter-/intra-granular precipitation mainly determined by composition and aging treatment; the localized deformation/fracture behaviour can be impacted by grain structures, indissoluble particles (e.g., Fe-bearing and S-Al₂CuMg phases) and precipitates^[3-5,7-9]. As a key stage of loading/fatigue failure, the micro-crack initiation/propagation can greatly determine the fatigue properties and fracture behaviour of high-strength aluminium alloys, which is widely underscored for the aerospace structural design, in addition to some external factors such as surface roughness, environment, load, etc.^[10-13] With appropriate composition design, the ways to control the microstructures such as grains/grain boundaries (GBs), precipitates, indissoluble particles enable the improved integrated properties of high-strength aluminium alloy plates.

Traditional processing route for high-strength aluminium alloy plates (i.e., symmetrical rolling (SR)), being limited by simplex plastic deformation mode, cannot obtain homogeneous through-thickness microstructures and properties^[14,15]. Increasing plate thickness makes it more difficult to tailor the appearance or formation of defects (e.g., inherited from casting),

coarse constituents, through-thickness uniformity, residual stress, etc., inescapably decreasing the integrated properties and servicing safety of the (mid-)thick plates^[9,11,16,17]. It seems that increasing the cast ingot thickness (that can increase the total reduction to the final thickness) or rolling reduction could to some extent enhance the penetration of deformation/strain into the plate centre for improving the through-thickness deformation/microstructure homogeneity. This route, however, may be limited by the available casting machines and rolling mills. The asymmetrical rolling (ASR) process can introduce additional shear deformation and cause so-called “cross rolling” zones that can help in penetrating the shear deformation into the plate centre, for improving through-thickness deformation distribution^[18]. This process has been shown to dramatically refine grains, weaken textures, improve through-thickness uniformities of microstructures and properties for Al-, Mg-, and Ti-based alloy sheets^[18-22]. The additional shear deformation, as the most attractive feature of ASR process, would be of particular interest for enhancing/improving the through-thickness deformation uniformity or, at least, alleviating the through-thickness deformation difference for (mid-)thick plates. However, the different metal flows between the upper and lower layers of the plates during ASR processing may ease plate bending, which could not only endanger the rolling mills but also affect the quality of rolled plates and multi-pass ASR processing^[23]. This bending behaviour can be suppressed or eliminated during rolling of thin sheets with tension coiling, which sadly cannot be implemented for (mid-)thick plates. Some simulations were performed to build relationship between bending behaviour and rolling parameters (i.e., speed ratios, reduction, mill diameter, etc.) in a bid to find a promising way to tackle this issue (i.e., eliminating or weakening the bending)^[23-28], which demonstrated some possibilities but without sufficient and convincing experimental evidence, especially for high-strength aluminium alloy plates.

With taking into account the individual influence of each ASR processing parameter on plate bending, it appears that multi-parameter, synergistically optimized ASR process may enable to tackle the bending problem and generate multi-pass ASR processing for aluminium alloy plates to improve through-thickness uniformities of deformation and microstructures^[29,30]. In spite of some remaining nonuniformity of through-thickness plastic deformation, the multi-pass ASR processing can effectively increase the deformation in the plate centre as compared to that of SR processing. This can promote the central microstructure evolution, such as the

grain structures, distribution of indissoluble particles along plate thickness, so as to positively affect the loading (also cycled) and failure behaviour of the final plates or components, which has not been addressed yet. In this investigation we study and evaluate the low cycle fatigue properties, fracture and failure behaviour of high-strength AA7050 aluminium alloy plates produced by multi-pass ASR processing with bending control^[30]. The effects of microstructure on the properties and future directions of research are discussed, aiming at the fundamental understanding of the ASR process for high-strength aluminium alloy plates.

2. Experimental procedure

Commercial hot-rolled AA7050 aluminium alloy plates with the original 50 mm thickness were homogenized at 475 °C for 24 h with air cooling to room temperature. The structure after that contained coarse grains and intermetallics (i. e., Al₇Cu₂Fe and S-Al₂CuMg particles, Fig. S1). Then, after holding at 400 °C for 1 h, the plates were SR-ed or ASR-ed with 5 passes (without lubrication): 50 mm → 35 mm → 25 mm → 18 mm → 14 mm → 10 mm, with 400 °C, 1 h annealing between passes. The rotating velocity of the top and bottom rollers were either 1 m/s both for SR process, or 0.8 m/s and 1 m/s for ASR process (speed ratio: 1.25), respectively, which represented optimised settings for multi-pass ASR process with bending control as described elsewhere^[30]. The rolled plates were one- or two-step annealed (recrystallized) at 445-475 °C for 0.5-2 h using an electric resistance furnace (see Supplementing Materials), and water quenched for microstructure observation. The samples for mechanical tests were solution treated at 475 °C for 1 h with water quenching and, after 2% stretching, were aged according to T74 regime: 120 °C, 6 h+163 °C, 24 h. The time interval between the solution and aging treatments was within 2 h.

The fatigue samples were cut along the rolling direction (RD) with flat clamped ends. The total sample length and width were 157 mm and 6.5 mm with middle 12 mm parallel segments. Room-temperature fatigue tests were carried out in an MTS-810 servohydraulic computer-controlled universal material testing machine with a strain level of 0.3-1.0 %, strain ratio $R = -1$ and the triangle load wave, according to GB/T 15248-2008 standard. The strain was controlled with a 10-mm extensometer (strain rate: $4 \times 10^3 \text{ s}^{-1}$). The duration of each test ensured three magnitudes (10^2 , 10^3 , 10^4 cycles) at each strain amplitude. Only one usable dataset for

each strain amplitude was collected by a computer during cyclic loading.

The present sample dimensions cannot meet the plane strain condition and the fracture toughness were assessed via measuring J-integral values based on load line compact tension (L-T direction). The pre-cracked samples (crack length: ~2 mm) were tensile tested in an MTS-810 universal material testing machine with a loading rate of 0.005 mm/min for obtaining force-crack open displacement curves for calculating J values based on GB/T 21143-2007 standard (ISO 12135: 2002, MOD).

According to GB 228.1-2010 standard (ISO 6892-1: 2009, MOD), at least two tensile samples (gauge length: 60 mm, width: 12 mm, thickness: ~10 mm) along RD for each plate were superficially smoothed and room-temperature tested in a universal material testing machine (200 KN) with a strain rate of $4 \times 10^3 \text{ s}^{-1}$ (see stress-strain curves in Fig. S2). The sample surfaces were mechanically polished before microhardness tests using a 401MVD microhardness tester with 0.2 kg load and 15 s loading duration. The values were averaged from 5 testing values excluding max and min values.

Samples for optical metallography (ZEISS Axio Imager A2m optical microscope) were polished using standard procedures and etched with Graff reagent (1 mL HF+16 mL HNO₃+3 g CrO₃+83 mL H₂O) for 40-45 s. A ZEISS SUPRA 55 field emission scanning electron microscope (SEM) and a Phenom XL Desktop SEM were used to observe the distribution of indissoluble particles, precipitates, grains and fractures. The microstructure statistics were obtained with ImageJ software (<https://imagej.net/>). The precipitates were observed by JEM-2100 transmission electron microscope (TEM, 200 KV) with selected area electron diffraction (SAED). TEM thin films were ground to ~80 μm thickness and twin-jet electro-polished with solution of 70% methanol and 30% nitric acid at -20 °C (voltage: 20 V, current: 80-100 mA).

3. Results

3.1 Low cycle fatigue properties and fracture toughness

The room-temperature tensile yield strength and ultimate tensile strength were measured (see Fig. S2) to be very close as 450 MPa and 506 MPa for SR plate while they are 440 MPa and 504 MPa for ASR plate, respectively, similar to those of AA7050-T7451 plate from AMS 4050 specification^[31]. Figure 1 shows that the typical stress-strain hysteresis loops at different

total strain amplitudes up to 0.6% for both plates display no plasticity or softening/hardening phenomena (except for slight plasticity at a strain amplitude of 0.6% that may be within the elastic deformation region). And obvious plasticity and strain hardening behaviour occur at strain amplitudes above 0.8% although the strain hardening level is decreased at 1.0% strain amplitude, similar to other aluminium alloys^[32,33]. The results also show that asymmetrical hysteresis loops appear at first cycle for a strain amplitude $\geq 0.8\%$ but disappears at stable and mid-life cycles. This could be associated with anisotropic plastic deformation behaviour during tension/compression for the complex grain structures or orientations. The “opening quarters” in the first-cycle hysteresis loops at higher strain amplitudes can be used to evaluate yield strength for both plates, i. e., at a strain amplitude of 1.0%, the ASR plate exhibits a higher yield strength (~ 390 MPa) than the SR plate (~ 375 MPa) although both values are lower than the monotonic tensile yield strength given in the beginning of this Section.

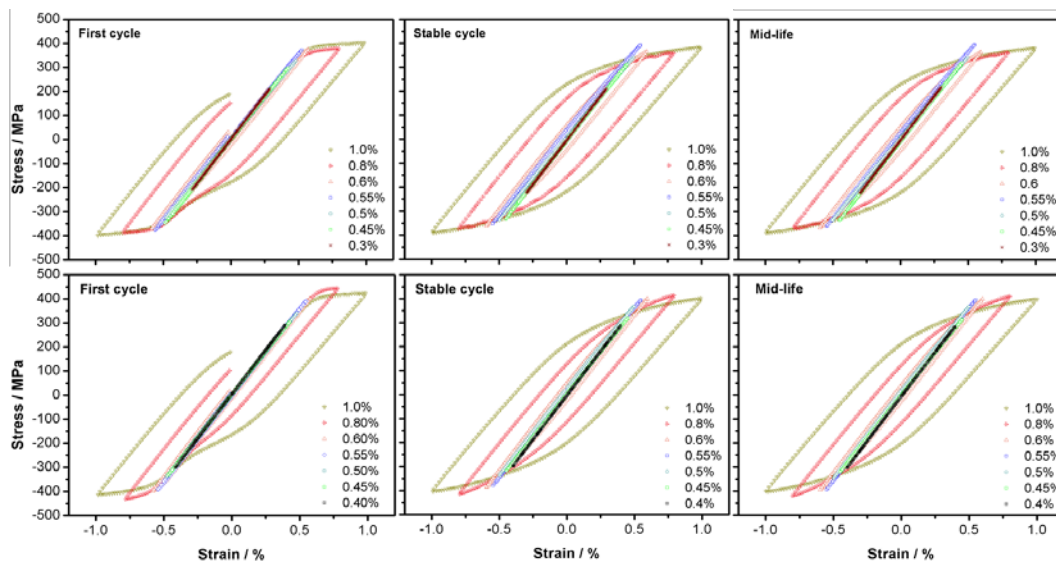


Fig. 1 Typical stress-strain hysteresis loops of the first, stable and mid-life cycles at different total strain amplitudes of the ASR (upper row) and SR (lower row) plates.

The stress/plastic strain amplitudes versus number of cycles at different total strain amplitudes for both plates are increased while their fatigue lives are diminished with the increasing total strain amplitudes, as shown in Fig. 2. The SR plate displays higher stress amplitudes including initial cyclic stress amplitudes for total strain amplitudes $\geq 0.5\%$, in comparison with ASR plate, although both exhibits almost similar stress amplitudes at a total

strain amplitude of 0.45%. Almost cyclic stabilization can be achieved after about $N_f=100$ for total strain amplitudes $\leq 0.5\%$, but cyclic softening and/or hardening behaviour occur at total strain amplitudes $\geq 0.55\%$ (both plates show similar stress amplitude at a total strain amplitude of 0.45%). For example, the stress amplitudes gradually decrease till the mid-life and then cyclic-hardened at a total strain amplitude of 0.55%, or continuous cyclic softening occurs at a total strain amplitude of 1.0% for both plates. This cyclic hardening/softening behaviour often occurs in aluminium alloys or others with coherent and shearable precipitates^[34-36]. These variations demonstrate that the SR plate with higher stress amplitudes exhibits better cyclic hardening ability at a total strain amplitude $\geq 0.55\%$ even if cyclic softening appears. For the plastic strain amplitude, the ASR plate displays higher values at total strain amplitudes of 0.8% and 1.0% that may be related with its higher tensile plasticity (Fig. S2), revealing possible significant plastic deformation during each loading at higher total strain amplitudes. Additionally, the loading elastic moduli are nearly constant with total strain amplitudes $\leq 0.6\%$ for SR plate and $\leq 0.8\%$ for ASR plate, further indicating that higher plasticity can be endured at higher total strain amplitudes. Thus, one can deduce that the higher tensile plasticity can contribute to better cyclic loading behaviour at higher total strain amplitudes, while the good hardening ability assures better cyclic loading behaviour at smaller total strain amplitudes. However, the fatigue life curves in Fig.3 indicate that the ASR plate exhibits a relatively low fatigue life at higher strain amplitudes ($\geq 0.8\%$) but almost similar fatigue life at low strain amplitudes ($\leq 0.6\%$) in comparison with SR plate. It is known that stronger materials could have longer fatigue life at low strain amplitudes and that high plasticity facilitates cyclically plastic deformation^[2,37,38], but it seems that the ASR plate with a higher plasticity does not display better fatigue endurance.

Then, the fatigue behaviour of both plates is assessed using total strain amplitude ($\Delta\varepsilon_t/2$) including elastic ($\Delta\varepsilon_e/2$) and plastic ($\Delta\varepsilon_p/2$) strain amplitudes, based on the combination of Basquin's equation and Coffin-Manson relationship, being suitable for high and low cycle fatigue regions^[37,39-41], respectively. The total strain amplitude can be calculated by eq. (1):

$$\frac{\Delta\varepsilon_t}{2} = \frac{\Delta\varepsilon_e}{2} + \frac{\Delta\varepsilon_p}{2} = \frac{\sigma'_f(2N_f)^b}{E} + \varepsilon'_f(2N_f)^c \quad (1)$$

where σ'_f is fatigue strength coefficient (MPa), ε'_f is fatigue ductility coefficient, b is fatigue

strength exponent and c is fatigue ductility exponent. Figure 4 (a, b) shows the elastic, plastic and total strain amplitudes as a function of the number of reversals to failure ($2N_f$), for which the stress/strain values at the mid-life cycles are used for ensuring a stable cyclic deformation. It demonstrates that the cyclic strain hardening exponent value n' of SR plate ($n'=0.0469$) is higher than that of ASR plate ($n'=0.0233$), revealing the former has a better cyclic hardening ability during cyclic loading. At the same time, cyclic stress-strain response as an important aspect that determines fatigue properties, can be used to understand the whole strain-controlled cyclic deformation behaviour, based on establishing the relationship between flow stress and plastic strain amplitude^[37,39-41] as follows:

$$\frac{\Delta\sigma}{2} = K' \left(\frac{\Delta\varepsilon_p}{2} \right)^{n'} \quad (2)$$

where K' is cyclic strength coefficient (MPa), n' is cyclic strain hardening exponent, with the mid-life stress amplitude ($\Delta\sigma/2$) and mid-life plastic strain amplitude ($\Delta\varepsilon_p/2$). The cyclic and monotonic stress-strain curves of both plates in Fig. 4 (c, d) show that the cyclic stresses match well with monotonic tensile stresses at smaller total strain amplitudes but are below the latter at higher total strain amplitudes ($\geq 0.8\%$). Additionally, Fig. 4 shows that the linear correlation coefficients for the elastic and total strain amplitudes are lower because of the limitation of Masson-Coffin relationship to describe strain-fatigue life curves. The cyclic stress-strain response also exhibits lower yielding and hardening behaviour than the monotonic response, which means that stress relaxation or cyclic softening occurs, especially at higher strain amplitudes, in accordance with the evolution of stress amplitude in Fig. 2.

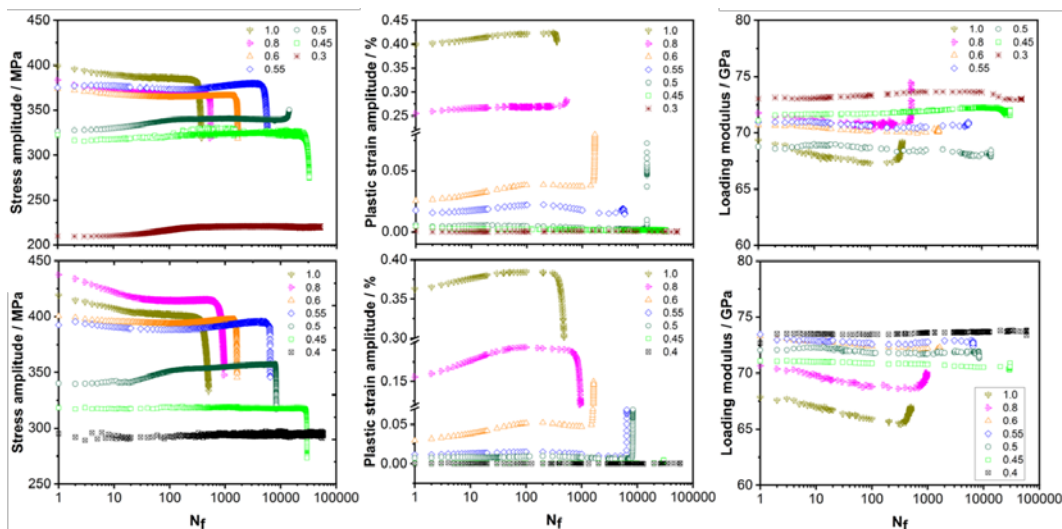


Fig.2 Stress/plastic strain amplitude and loading modulus versus number of cycles of the ASR

(upper row) and SR (lower row) plates at different total strain amplitudes.

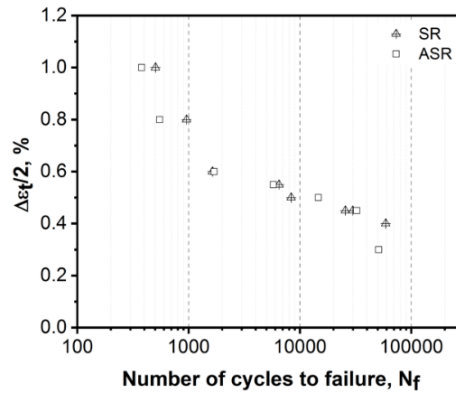


Fig.3 Fatigue life of both plates obtained at total strain amplitudes of 0.3-1.0%.

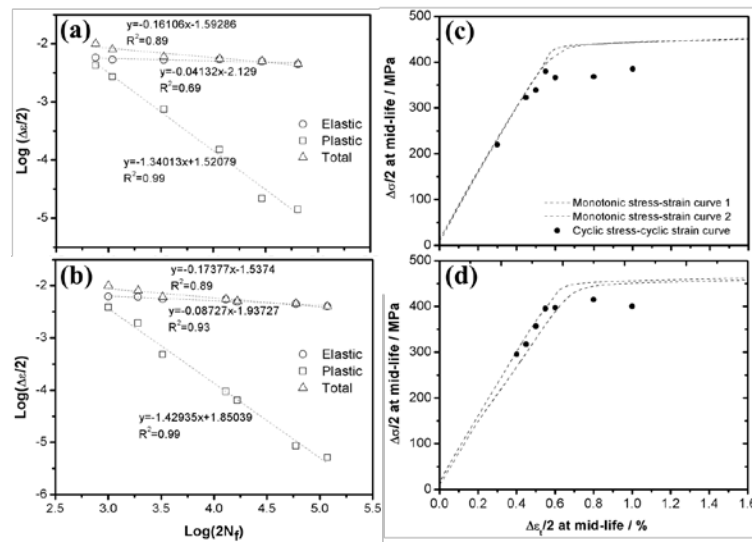


Fig.4 Strain life (a, b) and cyclic stress-cyclic strain curves (c, d) at mid-life cycles of ASR (a, c) and SR (b, d) plates. The typical monotonic tensile stress-strain curves at same strain rate $4 \times 10^{-3} \text{ s}^{-1}$ (two tests for each) are for comparison.

The experimental toughness results are shown in Table S1 and for $\Delta_a < 0.2 + (J_0 / (3.75\sigma_b))$ mm, F (the first maximum force during the test) and J_0 are recorded as F_c and $J_{c(B)}$. Under elastic-plasticity condition, the stress/strain level reaching the critical values near crack tips is determined via J integration and the unstable fracture is considered [2,38]. It is found that J_c of ASR plate ($33.8 \pm 0.2 \text{ kJ/m}^2$) is smaller than that of SR plate ($37.5 \pm 0.1 \text{ kJ/m}^2$), which means a lower fracture toughness of ASR plate. Under the critical condition, there is a relation between J_c and K_c (stress intensity factor)^[1,38]: $J_c = K_c^2 (1 - \nu^2) / E$ ($\nu = 0.33$: Poisson's ratio, $E = 72 \text{ GPa}$: Young's modulus), by which the critical K_c values under plane stress condition for both plates

are calculated as $52.2 \text{ MPa}\sqrt{\text{m}}$ (ASR) and $55.0 \text{ MPa}\sqrt{\text{m}}$ (SR). It is known that both J_c and K_c are sensitive to sample dimensions if the plane strain condition cannot meet, i.e. decrease with thickness reduction. Without considering this factor, the toughness discrepancies mainly depend on their microstructural differences.

3.2 Microstructures of SR and ASR plates

The annealed (recrystallised after rolling) microstructures reveal higher recrystallization degree (light-grey areas in Figs. S3-S4) in the upper and bottom layers (partially enlarged in Fig. 5 (a, a1, d, d1)) while less pronounced recrystallization in the central layers of both plates. It shows that the surface layer of ASR plate (Fig. 5 (a)) exhibits stronger recrystallisation and coarser grains compared to that of SR plate (Fig. 5 (d)), although some unrecrystallised areas surrounded by recrystallised grains still appear in both surface layers. This demonstrates that the surface layers of annealed (recrystallized) ASR plate could have more recrystallised grain boundaries or high angle grain boundaries (HAGBs). The dark-grey areas in Figs. S3-S4 and Fig. 5 are characterized as unrecrystallised areas or subgrains (see enlarged images in Fig. 5 (b, c1, c2, e, f1, f2)) with most subgrain sizes $< 5\text{-}6 \mu\text{m}$, in which more subgrains with size $< 2 \mu\text{m}$ are formed in the recrystallised SR plate (Fig. 5 (c3, f3)). Some fine recrystallised grains might be also formed in these dark-grey areas but they cannot be distinguished from subgrains for their comparable sizes. It seems that both plates display similar recrystallisation features along their thickness (Figs. S3-S4), but different recrystallisation fraction maybe present at different layers such as in the central layers (Fig. S7). The hardness tests indicate that the surface layers (140-150 HV) with almost recrystallized grains display 8-12 HV lower microhardness compared to other thickness layers ($160 \pm 1.5 \text{ HV}$): a lower hardness of recrystallized regions agrees with other studies^[42-44]. As a result, these fine subgrains or unrecrystallised areas can contribute to a better microhardness/strength, possibly resisting crack propagation for more cycles. This reveals that substantial subgrains can benefit fatigue properties even though qualitatively similar recrystallisation features appear along the plate thickness.

On the other hand, the indissoluble particles such as Fe-bearing and S phases retained in aluminium alloys after recrystallization are widely considered to be detrimental to the fatigue properties and toughness^[4,5,8,45,46]. In this study, the statistic amounts of these indissoluble particles in different layers (Figs. S5-S6) gradually decrease with raising annealing

(recrystallisation) temperatures and become minimum after 475 °C, 0.5 h treatment (Fig. S7). But there are more indissoluble particles in the upper and bottom layers than that in the central regions, and the ASR plate exhibits a higher content of indissoluble particles than SR plate. These indissoluble particles are identified mainly as flakelike Al_7Cu_2Fe and round S- Al_2CuMg phases (Fig. S8) with most of them less than 3 μm in size (Fig. S7, few > 3 μm), among which 60-80% are less than 1 μm (about half of those < 0.5 μm) and a few may be larger than 5 μm (i. e., particle a and b in Fig. S8). And the upper and bottom layers contain more of large indissoluble particles than the central region (Fig. S7). To conclude, the recrystallized ASR plates contain higher amounts of indissoluble particles along the thickness and more coarse ones in the upper/bottom layer compared with SR plates. These through-thickness microstructure changes mainly depend on the processing histories that can determine deformation/strain distribution or the stored deformation energies (e. g., defects) along the plate thickness^[47,48] as a driving force for recrystallisation, which will be discussed later.

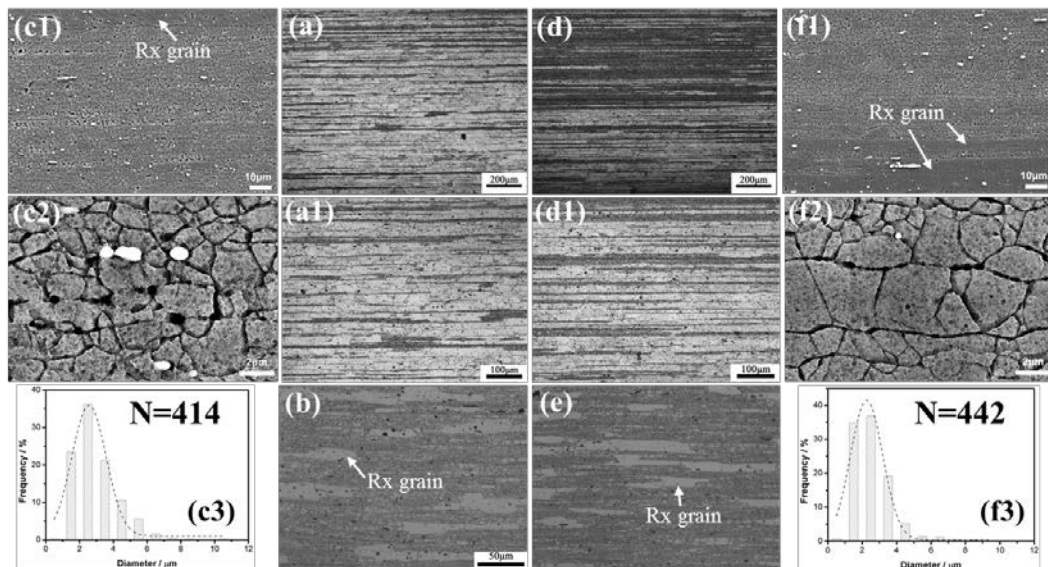


Fig. 5 Microstructures near the surface (a, a1, d, d1) and central (b, c1, c2, e, f1, f2) layers of ASR (a, a1, b, c1, c2) and SR (d, d1, e, f1, f2) plates after 475 °C, 1 h (a, a1, d, d1) and 475 °C, 0.5 h (b, c1, c2, e, f1, f2) treatments. (a1) and (d1) are magnified images of the local areas in (a) and (d), respectively. (b) and (e) are magnified images of central microstructures of ASR and SR plates. (c1, c2) and (f1, f2) are SEM images of local areas in (b) and (e), respectively, showing coarse recrystallized grains and fine subgrains. (d3) and (e3) are the statistic subgrain size distribution in ASR and SR plates with statistic numbers inserted. The

coarse recrystallised grains are marked as Rx grain. Dotted line: non-linear Gauss fitting curves. ((b) and (e) have same scale)

3.3 Low-cycle fatigue and toughness fractures

The fatigue fractures can reflect the irreversible deformation of metals induced by combined impacts of loads/stresses, defects, environment and other factors, which normally includes micro-crack initiation, propagation and final rupture stages^[2,38,49]. All the present fatigue fractures exhibit dark crack propagation region and relatively bright rapid rupture region, and the radial microstructural patterns appear inward from the surface in the crack propagation region, as shown in Figs. 6-9 (top-left). Multiple crack initiation sites appear at high strain levels (0.55%) but with a single dominant site (Figs. 8-9). For the ASR fatigue fracture at a strain level of 0.45%, Fig. 6 shows that A and B areas in its top-left image exhibit river-like patterns spreading into the centre (Fig. 6 (A1, B1)) and fatigue striations with micro-cracks white-marked in Fig. 6 (A2), which is directly related with the opening, closure and interaction of fatigue cracks^[49]. These features can also be seen in the crack propagation region of the SR fatigue fracture (Fig. 7 (A1)), as well as in the ASR fatigue fractures in Fig. 8. But the SR fatigue fractures in Figs. 7 and 9 show more facets or flat morphology, unlike the river-like patterns in Figs. 6 and 8. Fatigue striations (or steps) and localized cracking can be seen in Fig. 6 (A2, B2), Fig. 7 (A2, B1, B2) and Fig. 8 (A3, B), and the fatigue striations from the left to right in Fig. 6 (A2, B2) change propagation direction that may signify crack deflection when meeting different grains/subgrains (boundaries). GBs are considered as one of major obstacles to impede dislocation slip or transmission of slip bands^[50]. The fatigue striations cannot be easily found in Fig. 9 but some subtle fatigue propagation traces (white-marked in Fig. 9 (A2, E)) appear as well as fatigue steps in its B area (enlarged in Fig. 9 (B)), which belongs to fatigue propagation region with different morphology as compared to Figs. 6-8.

The fatigue striations or steps as severe localized deformation areas, tend to be early fractured or cracked under local overloading, as red-marked in Fig. 6 (A2, B2) and Fig. 7 (B2), which might develop into secondary micro-cracks with further fatigue. Additionally, the laminated boundaries corresponding to the elongated grains or subgrain boundaries (white-marked in Fig. 6 (A1, B1) and Fig. 8 (A1)) are usually decorated with indissoluble particles or GBPs (yellow-marked in Fig. 6 (A2, B2), Fig. 7 (A2, B3) and Fig. 8 (A2, A3)). These

boundaries might be cracked or fractured during cyclic loading, causing micro-cracks such as in Fig. 6 (A2), and exposing some brighter fine particles in front of the fatigue striations (yellow-marked in Fig. 7 (B3)) or on the fracture surface (yellow-marked in Fig. 8 (A3, B), < 1 μm). These demonstrates that the fatigue micro-cracking or crack propagation along GBs or subgrain boundaries is intimately connected with these fine particles (including GBPs). Some fractured short-rod phase (red-marked in Fig. 8 (A3)) and pits after particle debonding (white-marked in Fig. 8 (A3)) also can be seen. However, flocculent or fuzzy fracture areas (marked by white ellipsoids in Fig. 7 (B1), also in Fig. 7 (B2, B3)) maybe correlated with severe localized plastic deformation such as strong dislocation/defect interaction, causing entangled deformation defects and making the fracture front more intricate with fuzzy morphology. All the fatigue fractures exhibit final dimpled ductile rupture region (Fig. 6 (C2, D), Fig. 6 (D1, E2), Fig. 8 (D1, E1) and Fig. 9 (C)) after a transition from fatigue propagation region. Fig. 6 (C1) clearly shows a transient region C with fatigue striations on the left and dimples with embedded secondary particles on the right. Note that the transient region C in the SR fatigue fracture exhibits relatively flat morphology and larger-spaced fatigue striations along with partially cracked fatigue striations (red-marked in Fig. 7 (C)), which signifies approach to the end of fatigue propagation. Figure 9 (D) shows fracture morphology similar to that in Fig. 7 (B2) with fatigue striations in D area. To summarise: A to C areas in Fig. 6-8, and A, B, D and E areas in Fig. 9 belong to crack initiation and propagation regions while C to E areas in Fig. 6-8 as well as C area in Fig. 9 reflect the final rupture regions.

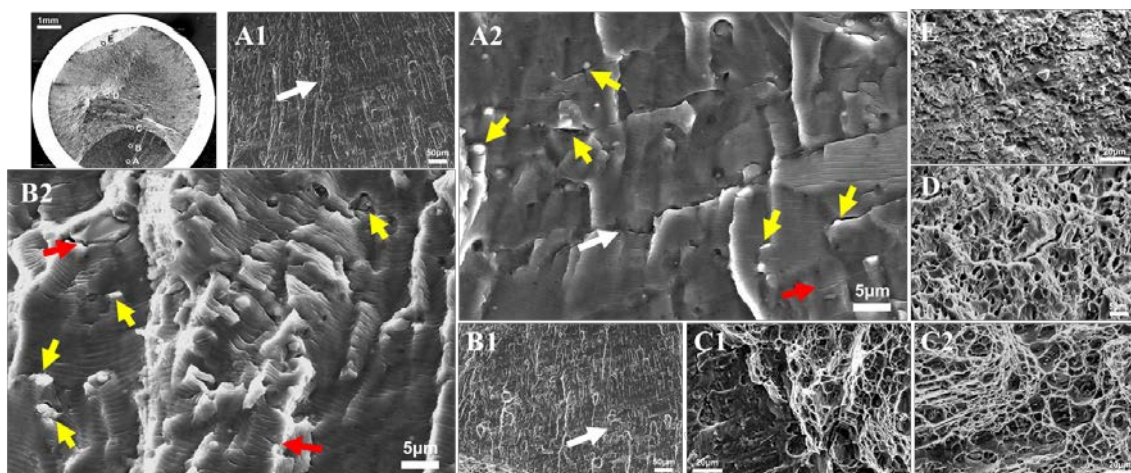


Fig.6 Fracture morphologies of A-E area in the ASR fatigue fracture (top-left) at a strain level of 0.45%. White arrows in (A1, A2, B1) show the direction of the elongated grains and some

(sub)grain boundaries. Red arrows in (A2, B2) indicate the cracking along fatigue striations while yellow arrows in (A2, B2) indicate bright finer particles and related micro-cracks.

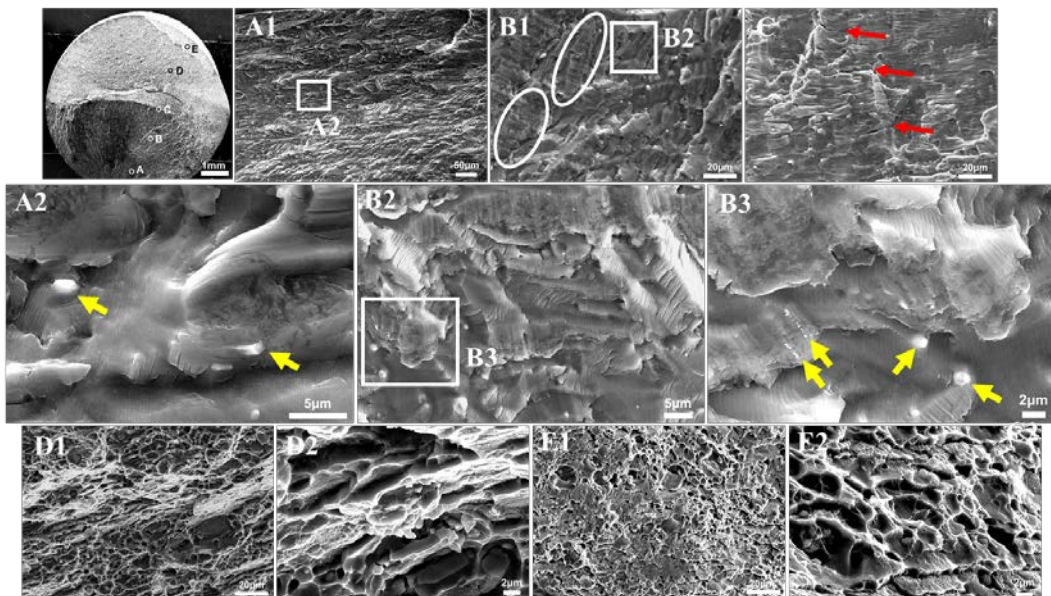


Fig.7 Fracture morphologies of A-E area in the SR fatigue fracture (top-left) at a strain level of 0.45%. Red arrows in (C) indicate the cracking along fatigue striations while yellow arrows in (A2, B3) show bright finer particles.

With above analysis, during fatigue of both plates, the fatigue crack initiation and propagation are inescapably affected by grain/subgrain boundaries and indissoluble particles or precipitates, including the contribution of debonding/cracking of particle-matrix interfaces and GBs. Following micro-crack propagation/coalescence, the fatigue resistance gradually decreases as the alloy cannot sustain more cycles. Furthermore, the A, B and C areas in Figs. 6 and 7 correspond to the initial, middle and later stages of crack propagation and their striation spacings are measured as: $0.42 \pm 0.01 \mu\text{m}$, $0.69 \pm 0.04 \mu\text{m}$, $0.73 \pm 0.06 \mu\text{m}$ for ASR fracture while $0.27 \pm 0.03 \mu\text{m}$, $0.39 \pm 0.03 \mu\text{m}$, $2.06 \pm 0.15 \mu\text{m}$ for SR fracture, respectively. According to the relationship between fatigue striation spacing and crack propagation rate^[2], these data show that the crack propagation rate in ASR plate is higher than that in SR plate from the initial to middle stages ($0.42 \mu\text{m}/\text{cycle}$ to $0.69 \mu\text{m}/\text{cycle}$) with similar propagation rate from middle to latter stages ($0.69 \mu\text{m}/\text{cycle}$ to $0.73 \mu\text{m}/\text{cycle}$). For SR plate, it is modestly increased from the initial to middle stages ($0.27 \mu\text{m}/\text{cycle}$ to $0.39 \mu\text{m}/\text{cycle}$) while sharply increased from middle to latter stages ($0.39 \mu\text{m}/\text{cycle}$ to $2.06 \mu\text{m}/\text{cycle}$). Figs. 6 and 7 further indicate when the crack

in SR plate approaches the middle stage, the crack propagation in ASR plate is finished and is getting into the final rupture region. To some extent, it reveals that the SR plate better resists the crack propagation than ASR plate, in accordance with their fatigue lives.

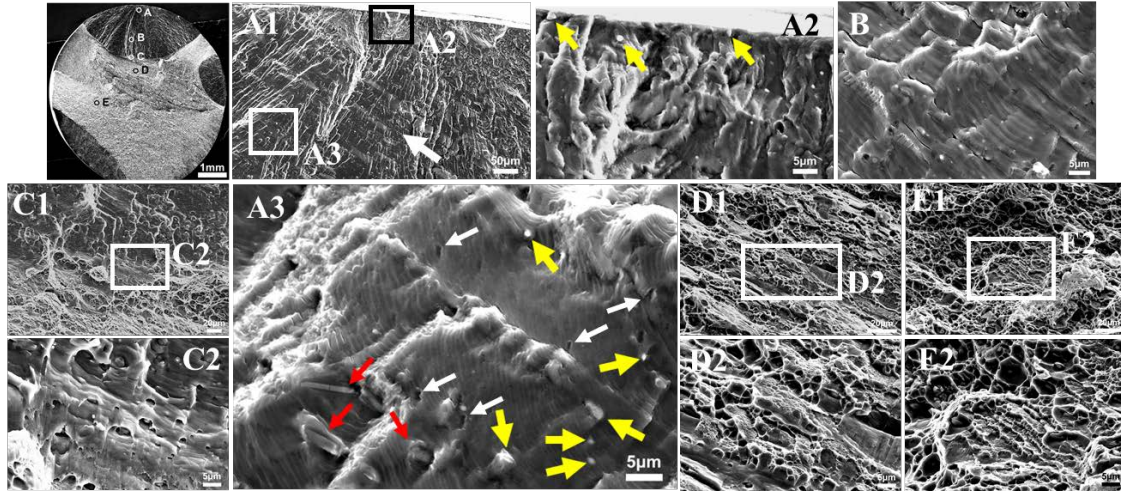


Fig.8 Fracture morphologies of A-E area in the ASR fatigue fracture (top-left) at a strain level of 0.55%. White arrow in (A1) shows the direction of the elongated grains while in (A3) white arrows show the pits after particle debonding. Yellow arrows in (A2, A3) show bright finer particles in front of fatigue cracks.

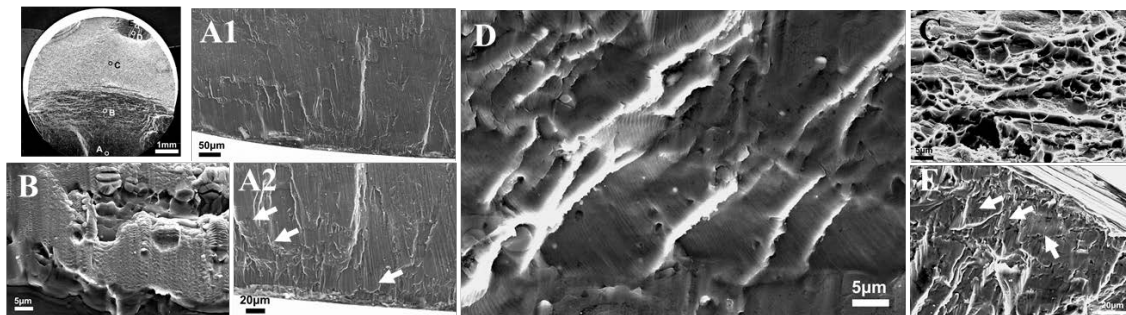


Fig.9 Fracture morphologies of A-E area in the SR fatigue fracture (top-left) at a strain level of 0.55%. White arrows show the micro-scaled fatigue striations.

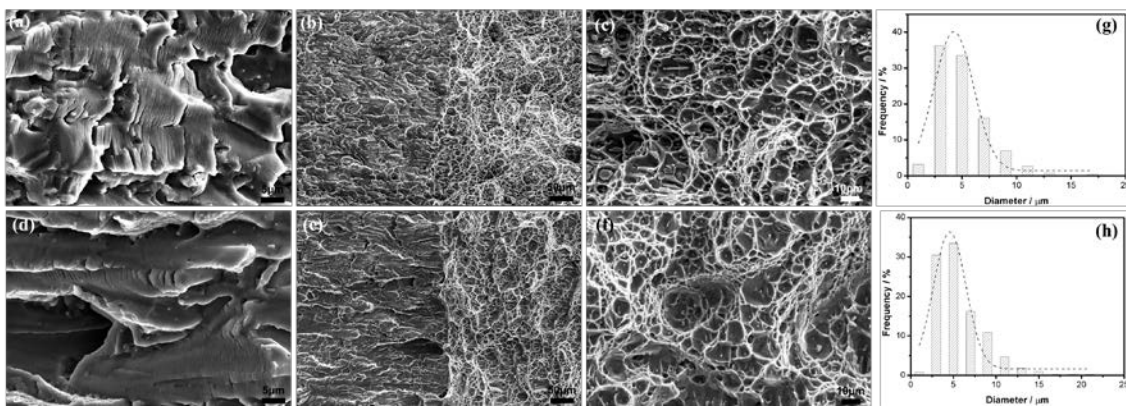


Fig.10 Toughness fractures of ASR (a-c) and SR (d-f) plates. (a) and (c) correspond to the left

and right of (b) while (d) and (f) correspond to the left and right of (e), respectively. (g) and (h) are the statistic dimple size distribution from ASR and SR toughness fractures, respectively. Dotted lines: non-linear Gauss fitting curves.

For both cases of toughness fractures, Fig. 10 (b, e) shows two main regions: fatigue pre-cracking (with more facets) and crack propagation regions. In the former region, the SR fracture exhibits obvious flat feature (Fig. 10 (d)) while the ASR fracture shows transgranular cleavage feature (Fig. 10 (a)) along with mutual fatigue striations that displays some micro-cracking (similar to that in Fig. 6 (B2) and Fig. 7 (C)). The spacing of fatigue striations are measured as $\sim 0.41 \pm 0.02 \mu\text{m}$ (ASR) and $\sim 0.21 \pm 0.02 \mu\text{m}$ (SR), which implies relatively rapid crack propagation in ASR plate ($0.41 \mu\text{m}/\text{cycle}$ vs $0.21 \mu\text{m}/\text{cycle}$ (SR)). The crack propagation region (Fig. 10 (c, f)) also exhibits dimpled ductile fracture with inner secondary particles. Both dimples ($< 10 \mu\text{m}$) seem comparable size distribution (Fig. 10 (g, h)), but the SR fracture contains larger dimples that represents better toughness, in line with above toughness tests.

4. Discussion

The above shows the changes of the fatigue behaviour of ASR and SR plates with increasing strain amplitudes and indicates that the SR plate displays better cyclic plastic deformation ability. However, during low-cyclic fatigue, low strain amplitudes correspond to low tensile or compressive deformation for each cycle that might be within the elastic deformation region, while the high strain amplitudes imply the occurrence of irreversible tensile or compressive deformation. For the repetitive tension/compressive deformations, the ASR plate with better tensile plasticity can intensify the strong defect interactions as well as local defect accumulation or annihilation. Whereas both plates undergo typical crack initiation, propagation and final rupture stages during low cycle fatigue, there may be different dependences on multiple factors such as microstructure, misorientation, loading condition^[3-6,8,10-13,16,17,51], especially effects of surface roughness, grain structure near surface on the crack initiation stage. The studied ASR and SR plates indeed display some microstructure and fracture differences. (1) After ASR/SR processing and subsequent annealing (recrystallisation), the primary coarse grains (Fig. S1) are replaced by partially recrystallised microstructures with

surface dominant recrystallised grains and central dominant unrecrystallised grains. Most subgrains are less than 6 μm in size while the SR plate has more subgrains with size $< 2 \mu\text{m}$. Also, the ASR plate has more recrystallised grains in the upper/bottom layer in comparison with that of SR plate. (2) Both plates have more indissoluble particles in their surface layers than their central layers and most refined indissoluble particles are less than 3-4 μm with only few $> 5 \mu\text{m}$ (Figs. S6-S7). The contents and sizes of those particles in the surface/central layer of ASR plate are higher/larger than that of SR plate (Fig. S7). (3) In the ductile fracture region, the SR plate shows more larger dimples, which is in accordance with its better toughness. (4) Obvious laminated grains and river-like patterns can be observed near the edge of ASR fatigue fracture, but the SR fatigue fracture exhibits more facets or flat morphology without observable laminated grain feature (5) In the fatigue crack propagation stage, the SR plate with narrower fatigue striation spacing exhibits relatively lower fatigue crack propagation rate or better fatigue crack propagation resistance. No obvious difference in the final rupture region can be found and no more explanation is given here considering its less importance for the fatigue life. The following will discuss the microstructure differences and their effects to fatigue crack initiation and propagation.

4.1 Reasoning for the microstructure differences of SR and ASR plates

As stated above, the microstructural differences such as in grain structures and distribution of indissoluble particles might be the critical factors to the fatigue behaviour of rolled plates. But those can be, in turn, highly affected by the deformation history such as the evolution of temperature, strain or deformation defects, which can greatly affect the annealing (recrystallisation) behaviour along plate thickness. The simulations in Figs. S9-S10 show that the through-thickness temperature distribution along the central line of SR- and ASR-ed plates are symmetric and asymmetric, respectively. Obvious temperature differences appear between surface and central layers in SR-ed plate (60-70 $^{\circ}\text{C}$ after pass 1-3), and between the upper and bottom layers as well as between surface and central layers in ASR-ed plate (40-50 $^{\circ}\text{C}$ after pass 1-3). The temperature near the upper layers of ASR-ed plates is always lower than at the bottom. The temperature differences are decreased after pass 4-5 SR/ASR processing, but which can still facilitate different plastic deformation or metallic flows across the plate thickness along rolling direction, leading to different deformation/strains and possible plate

bending, such as pass 5 ASR processing (Fig. S10), as also reported before^[30]. As a result, the asymmetric through-thickness distributions of compressive (ϵ_c) and shear (ϵ_s) strains occur in ASR plates, while they are symmetrically distributed in SR plates (Figs. S9-S10). As specifically shown in Fig. 11, although the ϵ_c is decreased from the bottom to upper layers, obviously higher ϵ_c is obtained after 5 passes ASR processing compared to 5 passes SR processing. This also can enhance the through-thickness difference of ϵ_c leading to significant plate bending. The through-thickness ϵ_s are almost similar after pass 1 and 2 of either SR or ASR processing, but strikingly increase in ASR after pass 3-5 as compared to the SR plate, further enlarging the through-thickness differences. The equivalent plastic strain ϵ_{eq} slowly diminishes from the bottom to upper layers in ASR plates and is higher in the bottom/central layer as compared to that of SR plate, but lower in the upper layer (e.g., after pass 3 and 4). Obviously, the ASR processing can efficiently enhance ϵ_s and ϵ_{eq} along plate thickness that facilitates microstructural deformation such as the refinement or fragmentation of grains and indissoluble particles, especially near the upper/bottom layer. However, highly recrystallised grains but not refined grains appear in the upper/bottom layers. This is associated with remarkable accumulated plastic deformations/strains near the upper/bottom layer that can accelerate the recrystallisation and result in coarse recrystallized grains. As a result, the ASR-ed plate has noticeable recrystallisation in its surface layer with higher ϵ_{eq} , which signifies that higher recrystallisation degree or coarser grains can be formed in ASR plate (i. e., bottom layer), as shown in Fig. 5 (a, a1). Meanwhile, for the severe plastic deformation near the upper/bottom layer, the deformation defects such as dislocations^[29] maybe highly accumulated, which will act as pipe diffusion paths to accelerate Cu and Mg solute diffusion during hot rolling and/or annealing (recrystallisation) treatments and promote growth/coarsening of constitutive particles such as S particle to larger ones (Figs. S5-S6). Also, relatively higher ϵ_{eq} in the central layer of ASR-ed plate could promote the coarsening of some particles. Therefore, controlling through-thickness deformation and annealing (recrystallisation) process in a bid to tailor recrystallisation degree, i.e. grain structures and constitutive particles, is pivotal to the integrated properties such as strength, toughness and fatigue properties as studied above.

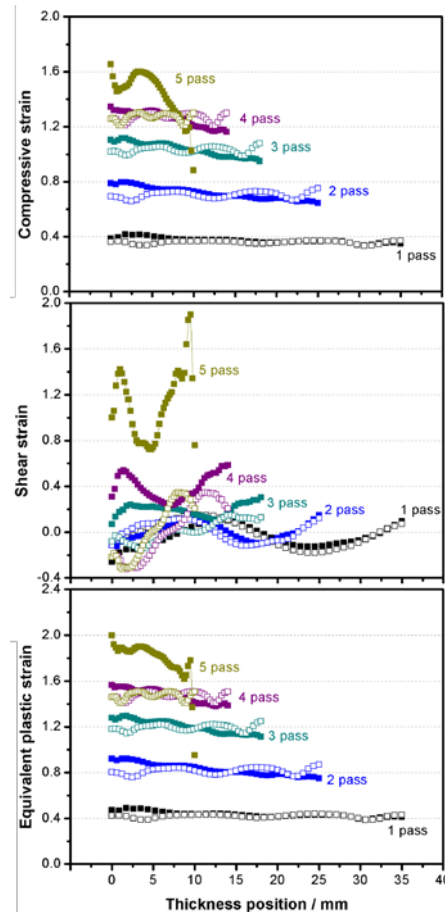


Fig.11 Through-thickness distribution of compressive, shear and equivalent plastic strains after each pass ASR and SR processing (the negative shear strain means opposite direction, zero point of thickness represents one side of plate. Solid circle: ASR, hollow circle: SR)

At present, a two-step annealing (recrystallization) treatment is used to control the recrystallization process: first step (445 °C, 2 h) for consuming the stored energies and decreasing the driving force of recrystallization, second step (475 °C, 0.5 h) for dissolving the secondary phases (i. e., η and S phases) and recrystallization. Figure S11 shows an observable decrease of the recrystallised areas from the surface to layers in the ASR plate as compared to SR plate. Figure S7 also indicates that the recrystallisation degree in the central layers of SR ($\sim 19.5 \pm 1.5\%$) and ASR ($\sim 18.8 \pm 1.2\%$) plates (Fig. S5) decreases as compared to those after one-step treatments (i. e., $\sim 21.1 \pm 1.1\%$ (SR) and $\sim 22.5 \pm 1.2\%$ (ASR) after 475 °C, 0.5 h treatment), along with similar through-thickness recrystallization features to Figs. S3-S4. And the amounts of remaining indissoluble particles in the central and surface layers become lower (Figs. S5-S6). We further changed the first step to 440 °C, 1.5 h with the same second step and

further decreased the recrystallisation degree of ASR plate to ~17.4%, lower than above values. Also, the number of indissoluble particles with sizes among 1-3 μm is apparently increased after two-step treatment (e. g., 445 °C, 2 h+475 °C, 0.5 h), and the ASR plate still has higher content of indissoluble particles (1-2 μm) in different layers (Fig. S7). This may be due to longer annealing (recrystallisation) times at high temperatures and seemingly reveals inevitable coarsening of indissoluble particles (i. e., S particle) under controlled recrystallization. It should be noted that the present SR and ASR processing are performed without lubrication and using small rolling mills in comparison with the industrial cases with lubrication and larger mills. This will cause heavy friction between rolling mills and plate surfaces that could enhance the deformation in the upper/bottom layers and promote the recrystallisation of the surface deformed microstructures during annealing (recrystallisation) treatments.

4.2 Correlating microstructures with fatigue loading behaviour and fracture

During early stage of fatigue, with loads less than the yield strength of an AA7050-T7451 aluminium alloy, the plastic deformation will be localized with complex dislocation interactions, such as slip bands^[2,38,52], leading to high tensile or compressive stress within slip bands and their adjacent areas^[2,38,53], which contributes to the early cyclic hardening (i. e., at low strain amplitudes in Fig. 2). The upper/bottom layers in both plates display coarse recrystallised grains, which are known to easily cause localized slip bands^[54,55]. As such, the repetitive intrusion and extrusion of slip bands as a key deformation feature of early fatigue can occur in the surface grains^[2,38,53], and the intrusion as a crack-like defect can initiate fatigue cracks^[53], i.e. being a crack initiation stage. Fig. 12 (a, b) shows obvious deformation traces or reliefs on sample surfaces as well as micro-cracks perpendicular to loading axis after certain cycles. From the longitudinal section adjacent to the edge of this fatigued sample, the deformed microstructures or some intrusions can be clearly seen (Fig. 12 (c)). Figs. 6-9 also indicate that the fatigue cracks are initiated near sample surfaces. Thus, it can be deduced that the localized deformation and formation of slip bands in surficial coarse recrystallised grains can promote preferential nucleation of fatigue cracks and early crack initiation^[54,55]. But slip bands will meet GBs and whether they can or cannot go through these GBs depends on obstacle strength of GBs or local stress states near GBs^[56-58]. Some considered that the slip bands are difficult to go through GBs with higher misorientation angles^[48,59], i. e. the surficial recrystallised grains

with HAGBs, which could facilitate the formation of slip bands but cannot let slip bands to go through. Especially in ASR plate, this will exacerbate early micro-crack formation and propagation along recrystallised GBs, reducing, to some extent, fatigue crack initiation life which usually accounts for ~90% of the total fatigue life^[60,61]. For the cyclic softening as shown in Fig. 2, the loss of localized hardening ability might be in charge of this^[36,62]. For instance, the accumulated high-density dislocations within slip bands as well as related strong shear deformation could repeatedly shear coherent precipitates^[62] such as η' phase or atomic clusters (GP zones), causing their refinement that cannot exert great strengthening action. Moreover, the higher stacking fault energy of aluminium alloys can promote cross slip within slip bands for local softening. These softening phenomena can easily sustain the accumulation of plastic deformation or damage along the slip bands that will further aggravate strain localization.

Certainly, it is considered that if the adjacent grains have soft orientation or higher Schmid factors, the slip bands can pass through GBs and get into the soft grains because of their easy dislocation activities^[63-65], preceding transgranular crack propagation. This can noticeably decrease fatigue crack propagation resistance, and the grains with small Schmid factors are suggested to enhance the fatigue life^[63,66,67]. The longitudinal section (Fig. 12 (d, e)) of one sample without fatigue failure indicate that the roughly flat crack is propagated along the direction perpendicular to loading axis, with transgranular fracture within recrystallized grains (Fig. 12 (d)) and both transgranular and intergranular fractures occur in subgrain areas (Fig. 12 (d, e)). Fig. 12 (f-k) further shows that transgranular (in coarse recrystallized grains and subgrains) and intergranular (along subgrain boundaries or recrystallized GBs) fractures occur during fatigue crack propagation in both plates. In the transient region with shear stresses, the cracks are deflected to easy-deform paths or areas, i. e., along GBs (Fig. 10 (j1, j2)) or subgrain boundaries. In turn, the crack is tilted relative to loading axis in the final rupture region (Fig. 10 (h, k)) along with abundant dimples (Fig. 6-9), mainly as dimpled ductile fracture. Thus, the unrecrystallised grains or subgrains with low angle grain boundaries (LAGBs) can facilitate the passing of slip bands into adjacent grains for continuous transgranular propagation. And the subgrain areas with higher strength/microhardness can not only exhibit better plastic deformation resistance but exert more complex localized plastic deformation or stresses to adjacent grains, causing transgranular propagation, possibly as local low-energy fracture path.

These transgranular fractures within recrystallized grains and subgrains are conducive to a lower crack propagation rate and increase fatigue cycles^[6,42,57,63,68,69]. At same time, it reveals that compared to ASR plate, the SR plate with more subgrains near surface layers could sustain more initiation cycles and in combination with relatively low crack propagation rate it could have better fatigue life. These findings tell that the localized plastic deformation such as the well-known from literature slip bands^[2,38,52] originated from surficial recrystallised grains can initiate surficial micro-cracks that will propagate inward via transgranular and intergranular modes. Until clear GB cracking occurs in transition areas, the sample cannot sustain additionally more cycles. Thus, the intrinsic grain structures play important role in the fatigue crack initiation and propagation.

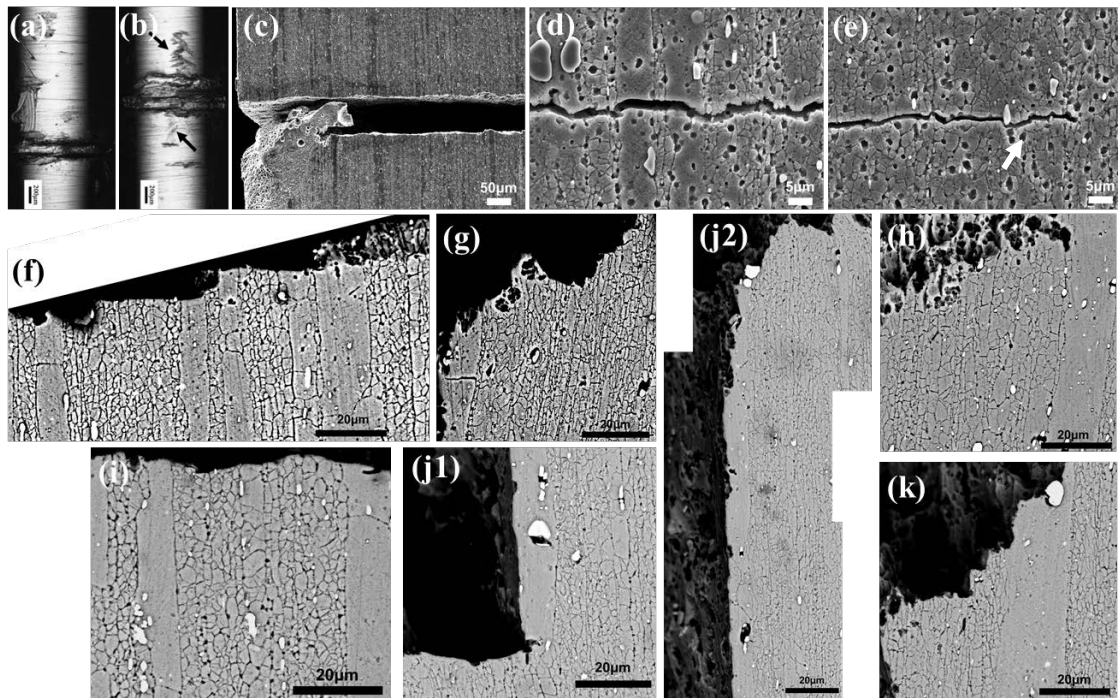


Fig.12 Surface morphologies of the fatigue ASR sample ((a), strain amplitude 0.30% and 50833 cycles) and SR sample ((b), strain amplitude 0.45% and 25493 cycles). Longitudinal section near sample surface (c) or close to the crack tip (d, e) of one sample without fatigue failure (strain amplitude 0.45%). Longitudinal-section microstructures near the fatigue fractures of the ASR (f-h) and SR (i-k) plates at a strain amplitude of 0.45%: (f, i) propagation region, (g, j1-j2) transient region, (h, k) final rupture region.

Figs. S5-S6 shows that the indissoluble particles are extensively fragmented or fractured

during/after SR and ASR processing compared to their original sizes in Fig. S1, but after subsequent annealing (recrystallisation) treatments, the ASR plate contains high amounts of indissoluble particles in its upper/bottom layer and higher proportion of larger particles with some $> 5 \mu\text{m}$ (Fig. S8). And coarse Fe-rich particles are commonly identified as possible crack initiation sites^[70,71]. Also, these indissoluble particles often present as local particle clusters or strings with partially containing remnant inner cracks, and the fatigue loading will cause further partial cracking of the indissoluble particles^[70]. These cracked indissoluble particles as well as their debonding with the matrix can easily become key micro-crack initiation sites with subsequently propagating into the matrix and bridging as larger cracks^[11,70,72]. The debonding between indissoluble particles and the matrix could facilitate crack deflection, as-marked in Fig. 12 (e), and may slightly decrease crack propagation rate. Thus, larger indissoluble particles with inner cracks in combination with surface recrystallised grains can further enhance the local crack initiation and premature crack development/propagation in ASR plate, signifying relatively shorter initiation stage that will cut down its fatigue life in comparison with SR plate.

4.3 Precipitate-related fracture analysis

Compared with indissoluble particles, the precipitates can induce different localized interaction with deformation defects (i. e., dislocations) that is associated with different monotonic/cyclic hardening abilities of metallic alloys^[44,45]. The AA7050-T7451 aluminium alloy usually contains coherent/semi-coherent η' phase and incoherent η phase (Fig. 13 (e, f)). Coherent η' particles in the matrix can be sheared by dislocations while semi-coherent η' precipitates and incoherent η particles will be bypassed leaving dislocation loops^[73]. Although the complex dislocation structures and severe plastic deformation within slip bands may promote reprecipitation of remaining solutes in the matrix of 7050-T7451 aluminium alloy, the limited local driving force for this reprecipitation may only cause formation of coherent clusters or GP zones, which still can be sheared. The shearing can facilitate both plane slip and strain localization. The accumulated dislocation loops around larger precipitates (i. e., η phase) may lead to high kinematic hardening, but the high stresses caused by these loops may lead to their dilapidation and nucleation of micro-defects^[74]. As a result, cyclic softening occurs as shown in Fig. 2. Although the GBs are identified as key obstacle to fatigue crack growth^[50], the fatigue cracks can still propagate intergranularly, especially along HAGBs^[6,75-78], which are usually

decorated with coarse GBPs and wide PFZs after aging (Figs. 13-14) facilitating micro-pore nucleation and strain localization near GBs or within PFZs^[3,6,68,72,78,79]. This can decrease intrinsic fatigue crack resistance and increase fatigue crack propagation rate^[5,96], commonly in (mid-)thick high-strength aluminium alloy plates^[81]. Thus, wide PFZs connected with surficial coarse recrystallised grains could be key strain localization areas or favourable paths for continuous advancement of slip bands, resultantly boosting intergranular cracking. Especially under shear stress, the cracking will be highly enhanced for a rapid crack propagation^[81], becoming critical factor to affect low-cycle fatigue resistance. It can be seen that the extensively coarse surficial recrystallised grains in ASR plates resulted from severer plastic deformation work against extending fatigue crack initiation stage.

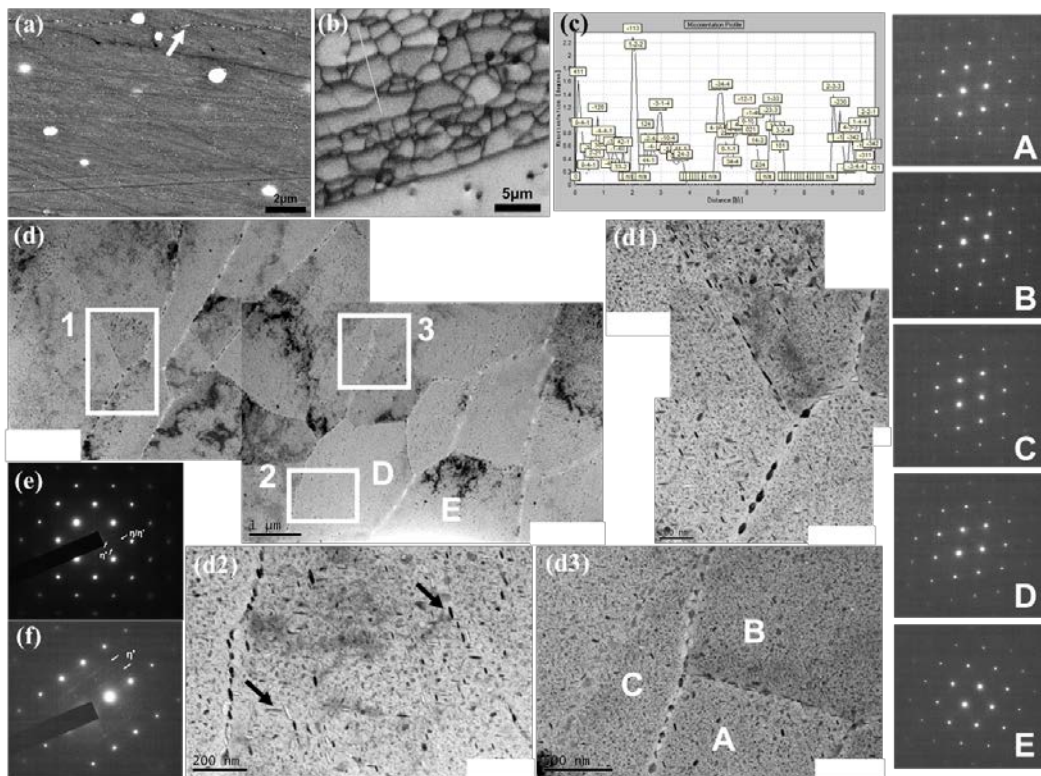


Fig.13 SEM (a) and TEM (d, d1-d3) images of the SR plate showing intragranular/intergranular precipitation. High-magnification images of region 1-3 correspond to (d1)-(d3), respectively. (b) orientation pattern quality map from local area, (c) point to point misorientation profile along white line in (b). (e) and (f) are SAED patterns along $[001]_{Al}$ and $[112]_{Al}$ axis, respectively. Note: some grinding scratches in (a). The SAED patterns of grain A-E are shown on the right, respectively.

The SEM characterizations in Fig. 13 (a, b) and Fig. 14 (a) show coarse precipitates along recrystallised GBs and fine ones along subgrain boundaries. The orientation maps and point to point misorientation profile (Fig. 13 (b, c)) reveal smaller misorientation angles among subgrains ($< 2.5^\circ$). Further TEM diffraction analysis indicates that the misorientation angles among A, B, C grains as well as between A and D grains are less than 2° , while it is 13.2° between D and E grains, whose GB is decorated with coarser GBPs and wider PFZ (Fig. 13 (d, d3)). Obviously, GB types as well as recrystallisation degrees are strongly connected with the sizes/morphologies of GBPs and PFZ widths, which agrees with reference data^[4,69,82]. The statistics show that in SR plate (Fig. 13) the GBP length, width and PFZ width along LAGBs are 25-65 nm, 7-16 nm and 35-50 nm, while those are 60-150 nm, 20-80 nm and 50-100 nm along HAGBs, respectively. In ASR plate (Fig. 14), these are 20-90 nm, 6-18 nm and 48-67 nm along LAGBs, while – 45-80 nm, 10-25 nm and 50-65 nm along HAGBs, respectively. Furthermore, as shown (black arrows) in region 2 in Fig. 13 and region 5 in Fig. 14, finer GBPs and inconspicuous PFZs appear along subgrain boundaries (LAGBs). The GBPs and partially larger short-rod precipitates in Figs. 13-14 correspond to stable η phase, along with uniform intragranular precipitate distribution. Also, the fine subgrains in Fig. 13 (a, d) and Fig. 14 (a-c) are in accordance with subgrains near the fatigue fractures (Figs. 12).

It is suggested that during cyclic loading the coherence of precipitates with the matrix can greatly affect crack propagation: the shearable (coherent) precipitates can boost the reversal slip of dislocations so as to decrease crack propagation rate, and the non-shearable precipitates (semi- and incoherent) can impede the reversal slip of dislocations that will result in dislocation accumulation near crack tips and accelerate crack propagation^[52,83]. For ASR plate, the obvious surficial recrystallized GBs (HAGBs) could impede the penetration of slip bands or dislocations across GBs. As a result, the localized deformation/strains occur and are gradually intensified along these GBs, especially within wide PFZs^[6,37,53,68,82], which can increase the probability of initiating and propagating surface micro-cracks. Combined with higher amounts of coarse indissoluble particles, the micro-cracks may be early nucleated and quickly gotten into the crack propagation stage. With increasing strain amplitudes, further enhanced interaction among dislocations, precipitates and GBs could enable strong localized deformation, causing short fatigue crack initiation stage in ASR plate following with cyclic softening, but it

still exhibits good fatigue resistance for a stable and durable interactions^[2]. Although the crack propagation could be encumbered by GBs^[42,43,84-86], the transgranular/intergranular fracture also appears in both crack propagation stages, conceivably consuming more fracture energy and benefiting the fatigue lives^[87,88].

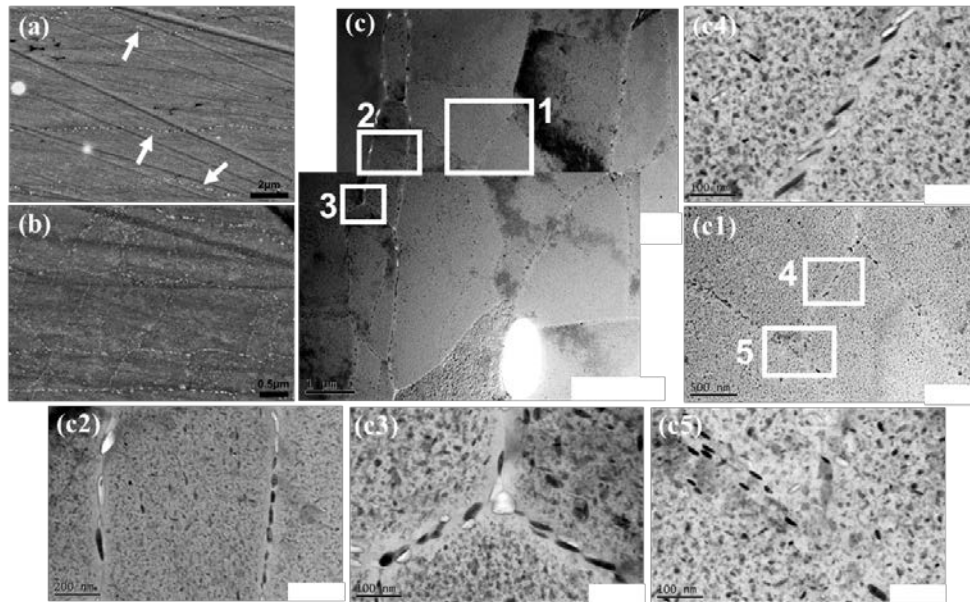


Fig.14 SEM (a, b) and TEM (c, c1-c5) images of the ASR plate showing intragranular precipitation and intergranular precipitation along HAGBs (as white-marked in (a)) and LAGBs (a, b). High-magnification images of regions 1-5 correspond to (c1-c5), respectively.

Note: some coarse or fine grinding scratches in (a).

Generally, the strong dislocation interaction and localized deformation lead to the formation of slip bands, within which the formation of local tensile and compressive stresses as well as their relaxation can primarily result in the repetitive intrusion/extrusion on sample surface^[53]. The ASR plate with plentiful recrystallised grains in its surface layers as well as relatively higher content of indissoluble particles, is prone to intensify the localized deformation such as intrusions as crack-like defects can initiate micro-cracks. In comparison with that of the SR plate, the ASR plate may have a shorter crack initiation stage that usually takes most of the total fatigue life. Furthermore, The SR plate exhibits smaller striation spacing or crack propagation rate, which is correlated with its finer subgrains and less indissoluble particles. Both plates display intragranular fracture within coarse recrystallised grains during crack propagation, but at the transition areas the intergranular fractures occur along HAGBs

and in turn accelerate crack propagation (Fig. 10 (g, j1, j2)). During this cyclic loading process, the coarse GBPs and related soft, wide PFZs along HAGBs or recrystallised GBs can expedite crack initiation and propagation, but the stronger subgrains, as better barriers, can retard rapid intergranular crack propagation that is desired for extending fatigue lives^[89-91].

4.4 Future research

The fatigue properties of high-strength aluminium alloys are impacted by intrinsic factors such as recrystallization or GB features, indissoluble particles, precipitates and PFZs, etc.^[4-6,12,44,57,84,71,78,92], which are closely connected to alloy composition, processing, heat treatment, etc. For partially recrystallised microstructures of high-strength aluminium alloys, the intergranular fracture seems inevitable, especially along HAGBs. With multiple-parameter synergistic action, the ASR processing can effectively improve the through-thickness shear/equivalent plastic strains. However, the related temperature and strain gradients can still impede uniform deformation along the plate thickness, causing higher strains and extensively coarse recrystallized grains in the surface layers as well as increased contents and sizes of indissoluble particles, which is obviously deleterious to fatigue loading. Additionally, the plate bending can occur during the ASR processing, i. e., after pass 5 ASR processing the bending occurs along with increased ε_s , which needs further modification of pass 5 ASR processing parameters. But almost no bending appears after pass 3 and 4 ASR processing (flat plates), in favour of a consecutive ASR process. Unfortunately, this makes the final ε_{eq} comparable to that of SR processing. It appears that the severer the plate bending, the higher the ε_s and/or ε_{eq} . With overcoming plate bending during ASR processing, the induced ε_s and their differences with that of the SR processing might be decreased, which makes it difficult to improve the central deformation and final through-thickness ε_{eq} . Hence, for increasing final ε_{eq} and its through-thickness uniformity, how to synergistically tailor the grain structures and recrystallisation (especially in surface and subsurface areas) becomes a critical issue for suppressing or delaying micro-crack initiation/propagation. In-depth studies should be devoted to tackle this inextricably technological and theoretical problems.

It is known that most high-strength aluminium alloys are produced with low impurity levels in a bid to decrease the content of undissolved particles as well as their detrimental impacts. But still, coarse indissoluble particles, inclusions (i.e., oxides) and other defects

cannot be avoided in the ingots/plates subject to industrial and composition designs, which can affect recrystallisation, micro-crack formation/propagation and fracture modes^[3-5,45,70,79,93]. For example, small debonding spacing and cracked particles could still facilitate the connection or coalescence of adjacent cracks for advancing crack propagation. Thus, besides of strict impurity element limitation, the size, distribution and morphology of indissoluble particles should be effectively controlled, especially the larger ones^[94], in order to decrease or mitigate their negative effect to the micro-crack formation. Lower impurity contents and effective purification treatment of aluminum melts combined with appropriate through-thickness deformation manipulation seem alternative way to control the coarse indissoluble particles.

The present T74 temper is mainly for improving corrosion resistance and cause larger precipitates such as stable η phase within grains that will decrease alloy's strength, but these larger precipitates can contribute to irreversible slip and uniform deformation. The accumulated dislocation loops around them may facilitate transgranular propagation if the slip bands or dislocations can penetrate adjacent grains with soft orientation or high Schmid factors. The unrecrystallised microstructures or subgrains with smaller GBPs, narrow PFZs and low GB orientation can improve fracture toughness and fatigue crack propagation resistance^[95], which are fully desired and may be achieved via feasible micro-alloying design and processing. For the precipitates, the extensively high-density semi-coherent η' phase could promisingly enable irreversible slip/uniform deformation for improving fatigue resistance and extending fatigue life while concurrently keeping high strength.

This study is originally targeted to tailor through-thickness grain structures using ASR processing featured with shear deformation, especially in the central layer, which is achieved. But still it enlarges the deformation/strain differences between the upper/bottom and central layers. This will cause rapid recrystallisation and grain growth during annealing (recrystallisation) treatments such as in the upper/bottom layer of ASR plate, which is unfavourable to improve fatigue crack propagation resistance and fatigue life. Modifying annealing (recrystallisation) treatments such as two-step process combined with effectual aging process (i. e., retrogression and reaging process) to obtain low recrystallisation degree, high-density semi-coherent precipitates as well as narrow PFZs and small GBPs, could decrease strain localization and increase fatigue crack propagation resistance for longer fatigue life. Thus,

optimizing integrated ASR processes including heat treatments as well as alloying design are eager to adjust through-thickness grain structures and localized GB features^[96-98] and, eventually, improve the final integrated properties of high-strength aluminium alloy plates.

5. Conclusion

The room-temperature low cycle fatigue lives of SR and ASR plates are decreased with increasing strain amplitudes, but the SR plate has better fatigue life and relatively better fracture toughness. This study shows that the fatigue micro-cracks are initiated from the surficial coarse recrystallised grains and the constitutive particles facilitate the local micro-crack formation and fatigue crack propagation. For the severe plastic deformation in the upper/bottom layer that could greatly increase the recrystallisation driving force, obvious surficial recrystallized grains as well as higher content of indissoluble particles (including more of larger ones) in the ASR plate could contribute to early crack initiation, subsequently leading to a shorter crack initiation stage as compared to that of SR plate. The SR plate with relatively weak surficial recrystallisation microstructures, finer subgrains and less coarse indissoluble particles resists better the crack initiation and propagation, expectantly generating better fatigue property.

It is concluded that the surficial recrystallised grains usually decorated with coarse GBPs and wide PFZs can easily be deformed and also contribute to more localised plastic deformation near GBs, which could promote the occurrence of intergranular fractures and crack propagation. Whereas, abundant subgrain areas (LAGBs) with fine GBPs, narrow PFZs and low GB orientation could enhance the energy-intensive transgranular fracture, enabling better cyclic loading behaviour and extending fatigue life. For pursuing a longer low cycle fatigue life, the through-thickness deformation or strain uniformity, recrystallisation as well as bending should be well balanced via optimizing integrated ASR processing including favourable annealing/recrystallisation and aging treatments, concurrently achieving more fracture-resistance microstructures such as subgrains/LAGBs and extensive intragranular semi-coherent precipitates. This might be a great challenge and dedicated efforts are required for technological and theoretical progress of the ASR processing.

Acknowledgement

The authors would like to acknowledge the financial support from the Major State Research and

Development Program of China (No. 2016YFB0300801), the State Key Laboratory for Advanced Metals and Materials of China (No. 2018Z-23) and the Constructed Project for Key Laboratory of Beijing, China. L.G., C. M., L. Z. and J. S. are grateful for the supports from International S&T Cooperation Projects of Nanjing, China (No. 201818014). L.G. and D. E. kindly acknowledge support from BCAST for hosting L.G.. L. G. thanks support from the China Scholarship Council (CSC).

Reference

- [1] Kaufman J G. Fracture resistance of aluminum alloys: notch toughness, tear resistance, and fracture toughness. ASM Int., 2001.
- [2] Suresh S. Fatigue of materials. Cambridge University Press, 1998.
- [3] Dumont D, Deschamps A, Brechet Y. On the relationship between microstructure, strength and toughness in AA 7050 aluminum alloy. Mater. Sci. Eng. A, 2003, 356 (1-2): 326-336.
- [4] Telesman J. Review of effects of microstructure on fatigue in aluminum alloys. NASA Technical Memorandum 83626, Apr. 1984.
- [5] Staley J T. How microstructure affects fatigue and fracture of aluminum alloys. In: Peronne N, editor. Tenth Symp. Naval Struct. Mech., Washington D. C., University Press; 1978, p. 671-684.
- [6] Pardoën T, Dumont D, Deschamps A, et al. Grain boundary versus transgranular ductile failure. J. Mech. Phys. Solids, 2003, 51 (4): 637-665.
- [7] Thompson A W, Backofen W A. The effect of grain size on fatigue. Acta Metall., 1971, 19 (7): 597-606.
- [8] Vasudevan A K, Sadananda R K. Role of microstructures on the growth of long fatigue cracks. Int. J. Fatigue, 1997, 19 (93): 151-159.
- [9] Harlow D G, Nardiello J, Payne J. The effect of constituent particles in aluminum alloys on fatigue damage evolution: Statistical observations. Int. J. Fatigue, 2010, 32 (3): 505-511.
- [10] Ray A, Patankar R. Fatigue crack growth under variable variable-amplitude loading: part I - model formulation in state-space setting. Appl. Math. Model., 2001, 25 (11):979-994.
- [11] Noroozi A H, Glinka G, Lambert S. Study of the stress ratio effects on fatigue crack growth using the unified two-parameter fatigue crack growth driving force. Int. J. Fatigue, 2007, 29 (9): 1616-1633.
- [12] Suresh S, Vasudévan A K, Bretz P E. Mechanisms of slow fatigue crack growth in high strength aluminum alloys: role of microstructure and environment. Metall. Trans. A, 1984, 15: 369-379.
- [13] Braun R. Transgranular environment-induced cracking of 7050 aluminium alloy under cyclic loading conditions at low frequencies. Int. J. Fatigue, 2008, 30: 1827-1837.
- [14] Salazar-Guapuriche M, Zhao Y Y, Pitman A, et al. Variations of properties across plate thickness for Al alloy 7010. Trans. Nonferrous Met. Soc. China, 2005, 15 (6): 1258-1263.
- [15] She H, Shu D, Wang J, et al. Influence of multi-microstructural alterations on tensile property inhomogeneity of 7055 aluminum alloy medium thick plate. Mater. Character., 2016, 113: 189-197.
- [16] Gao Y X, Yi J Z, Lee P D, et al. A micro-cell model of the effect of microstructure and defects on fatigue resistance in cast aluminum alloys. Acta Mater., 2004, 52 (19): 5435-5449.
- [17] Magnussen P E, Bucci R J, Hinkle A J, et al. Analysis and prediction of microstructural effects on long-term fatigue performance of an aluminum aerospace alloy. Int. J. Fatigue, 1997, 19 (93): 275-283.
- [18] Cui Q, Ohori K. Grain refinement of high purity aluminium by asymmetric rolling. Mater. Sci. Tech., 2000, 16 (10): 1095-1101.
- [19] Kang S B, Min B K, Kim H W. Effect of asymmetric rolling on the texture and mechanical properties of AA6111-aluminum sheet. Metall. Mater. Trans. A, 2005, 36 (11): 3141-3149.
- [20] Sidor J, Petrov R H, Kestens L A I. Deformation, recrystallization and plastic anisotropy of

- asymmetrically rolled aluminum sheets. *Mater. Sci. Eng. A*, 2010, 528 (1): 413-424.
- [21] Kim W J, Lee J B, Kim W Y, et al. Microstructure and mechanical properties of Mg-Al-Zn alloy sheets severely deformed by asymmetrical rolling. *Scripta Mater.*, 2007, 56 (4): 309-312.
- [22] Kim W J, Yoo S J, Lee J B. Microstructure and mechanical properties of pure Ti processed by high-ratio differential speed rolling at room temperature. *Scripta Mater.*, 2010, 62 (7): 451-454.
- [23] Anders D, Munker T, Artel J, et al. A dimensional analysis of front-end bending in plate rolling applications. *J. Mater. Proc. Tech.*, 2012, 212 (6): 1387-1398.
- [24] Park B H, Hwang S M. Analysis of front end bending in plate rolling by the finite element method. *Trans. ASME*, 1997, 119: 314-323.
- [25] Kiefer T, Kugi A. An analytical approach for modelling asymmetrical hot rolling of heavy plates. *Math. Comp. Model. Dyna. Syst.*, 2008, 14: 249-267.
- [26] Yoshii M, Ohmori K, Seto T, et al. Analysis of warping phenomenon in plate rolling. *ISIJ Int.*, 1991, 31 (9): 973-978.
- [27] Philipp M, Schwenzfeier W, Fischer F D, et al. Front end bending in plate rolling influenced by circumferential speed mismatch and geometry. *J. Mater. Proc. Tech.*, 2007, 184 (1-3): 224-232.
- [28] Lu J S, Harrer O K, Schwenzfeier W, et al. Analysis of the bending of the rolling material in asymmetrical sheet rolling. *Int. J. Mech. Sci.*, 2000, 42(1): 49-61.
- [29] Ma C Q, Hou L G, Zhang J S, et al. Influence of thickness reduction per pass on strain, microstructures and mechanical properties of 7050 Al alloy sheet processed by asymmetric rolling. *Mater. Sci. Eng. A*, 2016, 650: 454-468.
- [30] Ma C Q, Hou L G, Zhang J S, et al. Microstructures and properties of asymmetrical rolled 7050 Al alloy plate with bending behavior optimization. *Mater. Sci. Eng. A*, 2016, 657: 322-330.
- [31] AMS4050: Aluminum Alloy, Plate 6.2Zn-2.3Cu-2.2Mg-0.12Zr (7050-T7451) Solution Heat Treated, Stress Relieved, and Overaged, Dec., 1974. DOI: <https://doi.org/10.4271/AMS4050>.
- [32] Xue Y, McDowell D L, Horstemeyer M F, et al. Microstructure-based multistage fatigue modelling of aluminum alloy 7075-T651. *Eng. Frac. Mech.*, 2007, 74(17): 2810-2823.
- [33] Cisco A R, Jordon J B, Avery D Z, et al. Characterization of fatigue behavior of Al-Li alloy 2099. *Mater. Character.*, 2019, 151: 496-505.
- [34] Lee J K, Bhat S P, Veaux R, Laird C. Mechanisms of cyclic softening in precipitation-hardening alloys - A ball model approach and tests at 78 K. *Int. J. Fract.*, 1981, 17: 121-141.
- [35] Vogel W, Wilhelm M, Gerold V. Persistent slip bands in fatigued peak aged Al-Zn-Mg single crystals. I. Development of dislocation microstructure and change of precipitation distribution. *Acta Metall.*, 1982, 30: 21-30.
- [36] Srivatsan T S. Mechanisms governing cyclic deformation and failure during elevated temperature fatigue of aluminum alloy 7055. *Int. J. Fatigue*, 1999, 21: 557-569.
- [37] Li D M, Nam W J, Lee C S. A strain energy-based approach to the low-cycle fatigue damage mechanism in a high-strength spring steel. *Metall. Mater. Trans. A*, 1998, 29: 1431-1439.
- [38] Pokluda J, Šandera P. *Micromechanisms of Fracture and Fatigue*. Springer, 2010.
- [39] Song M S, Kong Y Y, Ran M W, et al. Cyclic stress-strain behavior and low cycle fatigue life of cast A356 alloys. *Int. J. Fatigue*, 2011, 33: 1600-1607.
- [40] Tong X Y, Wang D J, Xu H. Investigation of cyclic hysteresis energy in fatigue failure process. *Int. J. Fatigue*, 1989, 11 (5): 353-359.
- [41] Sarkar P P, De P S, Dhua S K, et al. Strain energy based low cycle fatigue damage analysis in a plain C-Mn rail steel. *Mater. Sci. Eng. A*, 2017, 707: 125-135.

- [42] Watanabe T, Tsurekawa S. The control of brittleness and development of desirable mechanical properties in polycrystalline systems by grain boundary engineering. *Acta Mater.*, 1999, 47(15-16): 4171-4185.
- [43] Jawad F F, Zikry M A. The Effects of grain-boundary orientations on failure behavior in F.C.C. polycrystalline systems. *Int. J. Damage Mech.*, 2009, 18(4): 341-369.
- [44] Morere B, Ehrström J C, Gregson P J, et al. Microstructural effects on fracture toughness in AA7010 plate. *Metall. Mater. Trans. A*, 2000, 31 (10): 2503-2515.
- [45] Deshpande N U, Gokhale A M, Denzer D K, et al. Relationship between fracture toughness, fracture path, and microstructure of 7050 aluminum alloy: part I. quantitative characterization. *Metall. Mater. Trans. A*, 1998, 29: 1191-1201.
- [46] Santner J S, Eylon D. Fatigue behavior and failure mechanisms of modified 7075 aluminum alloys. *Metall. Trans. A*, 1979, 10 (7): 841-848.
- [47] Doherty R D. Recrystallization and texture. *Prog. Mater. Sci.*, 1997, 42: 39-58.
- [48] Humphreys F J, Hatherly M. Recrystallization and related annealing phenomena. Pergamon, 2004.
- [49] Zhang X L, Zhang Z, Tao C H. Fatigue fractography quantitative analysis. National Defense Industry Press, 2010.
- [50] Merati A. A study of nucleation and fatigue behavior of an aerospace aluminum alloy 2024-T3. *Int. J. Fatigue*, 2005, 27 (1): 33-44.
- [51] Jian H, Jiang F, Wei L, et al. Crystallographic mechanism for crack propagation in the T7451 Al-Zn-Mg-Cu alloy. *Mater. Sci. Eng. A*, 2010, 527 (21-22): 5879-5882.
- [52] Ho H S, Risbet M, Feaugas X. On the unified view of contribution plastic strain to cyclic crack initiation: impact of the progressive transformation of shear bands to persistent slip bands. *Acta Mater.*, 2015, 85: 155-167.
- [53] Polák J, Man J. Fatigue crack initiation - the role of point defects. *Int. J. Fatigue*, 2014, 65: 18-27.
- [54] Lin F S, Starke Jr E A. The effect of copper content and degree of recrystallization on the fatigue resistance of 7XXX-type aluminum alloys - I. Low cycle corrosion fatigue. *Mater. Sci. Eng.*, 1979, 39 (1): 27-41.
- [55] Zhai T, Jiang X P, Li J X, et al. The grain boundary geometry for optimum resistance to growth of short fatigue cracks in high strength Al-alloys. *Int. J. Fatigue*, 2005, 27 (10-12): 1202-1209.
- [56] Cheng Y, Mrovec M, Gumbsch P. Atomistic simulations of interactions between the $1/2\langle 111 \rangle$ edge dislocation and symmetric tilt grain boundaries in tungsten. *Phil. Mag.*, 2008, 88: 547-60.
- [57] Wen W, Pei Cai P, Ngan A H W, et al. An experimental methodology to quantify the resistance of grain boundaries to fatigue crack growth in an AA2024 T351 Al-Cu Alloy. *Mater. Sci. Eng. A*, 2016, 666: 288-296.
- [58] Sperry R, Harte A, Fonseca J Q da, et al. Slip band characteristics in the presence of grain boundaries in nickel-based superalloy. *Acta Mater.*, 2020, 193: 229-238.
- [59] Liu Z, Guo X, Cui H, et al. Role of misorientation in fatigue crack growth behavior for NG-TIG welded joint of Ni-based alloy. *Mater. Sci. Eng. A*, 2018, 710: 151-163.
- [60] Murakami Y, Nomoto T, Ueda T, et al. On the mechanism of fatigue failure in the superlong life regime ($N > 10^7$ cycles). Part II: influence of hydrogen trapped by inclusions. *Fatigue Fract. Eng. Mater. Struct.*, 2000, 23: 903-910.
- [61] Li Y D, Zhang L L, Fei Y H, et al. On the formation mechanisms of fine granular area (FGA) on the fracture surface for high strength steels in the VHCF regime. *Int. J. Fatigue*, 2016, 82: 402-410.
- [62] Cervellon A, Hémerly S, Kürnsteiner P, et al. Crack initiation mechanisms during very high cycle fatigue

- of Ni-based single crystal superalloys at high temperature. *Acta Mater.*, 2020, 188: 131-144.
- [63] Zhai T, Wilkinson A J, Martin J W. A crystallographic mechanism for fatigue crack propagation through grain boundaries. *Acta Mater.*, 2000, 48: 4917-4927.
- [64] Shen F, Yi D, Jiang Y, et al. Semi-quantitative evaluation of texture components and fatigue properties in 2524 T3 aluminum alloy sheets. *Mater. Sci. Eng. A*, 2016, 657: 15-25.
- [65] Li F D, Liu Z. Y, Wu W. T, et al. Slip band formation in plastic deformation zone at crack tip in fatigue stage II of 2xxx aluminum alloys. *Int. J. Fatigue*, 2016, 91: 68-78.
- [66] Spangenberg A G, Lados D A, Coleman M, et al. Microstructural mechanisms and advanced characterization of long and small fatigue crack growth in cast A356-T61 aluminum alloys. *Int. J. Fatigue*, 2017, 97: 202-213.
- [67] Ma M Y, Wang B, Liu H Q, et al. Investigation of fatigue crack propagation behavior of 5083 aluminum alloy under various stress ratios: Role of grain boundary and Schmid factor. *Mater. Sci. Eng. A*, 2020, 773: 138871.
- [68] Gräf M, Hornbogen E. Observation of ductile intercrystalline fracture of an Al-Zn-Mg-alloy. *Acta Metall.*, 1977, 25 (8): 883-889.
- [69] Vasudevan A K, Doherty R D. Grain boundary ductile fracture in precipitation hardened aluminum alloys. *Acta Metall.*, 1987, 35 (6): 1193-1219.
- [70] Payne J, Welsh G, Christ R J Jr, et al. Observations of fatigue crack initiation in 7075-T651. *Int. J. Fatigue*, 2010, 32: 247-255.
- [71] Xue Y, El Kadiri H, Horstemeyer M F, et al. Micromechanisms of multistage fatigue crack growth in a high-strength aluminum alloy. *Acta Mater.*, 2007, 55(6): 1975-1984.
- [72] Ludtka G M, Laughlin D E. The influence of microstructure and strength on the fracture mode and toughness of 7XXX series aluminum alloys. *Metall. Trans. A*, 1982, 13: 411-425.
- [73] Mahon G J, Howe J M, Vasudevan A K. Microstructural development and the effect of interfacial precipitation on the tensile properties of an aluminum/silicon-carbide composite. *Acta Metall*, 1990, 38: 1503-1524.
- [74] León-Cázares F D, Monni F, Jackson T, et al. Stress response and microstructural evolution of nickel-based superalloys during low cycle fatigue: physics-based modelling of cyclic hardening and softening. *Int. J. Plasticity*, 2020, 128: 102682.
- [75] Tra T H, Okazaki M, Suzuki K. Fatigue crack propagation behavior in friction stir welding of AA6063-T5: Roles of residual stress and microstructure. *Int. J. Fatigue*, 2012, 43: 23-29.
- [76] Watanabe T. Grain boundary engineering: historical perspective and future prospects. *J. Mater. Sci.*, 2011;46: 4095-115.
- [77] Bechtel S, Kumar M, Somerday B P, et al. Grain-boundary engineering markedly reduces susceptibility to intergranular hydrogen embrittlement in metallic materials. *Acta Mater.*, 2009, 57: 4148-4157.
- [78] Kamp N, Gao N, Starink M J. et al. Influence of grain structure and slip planarity on fatigue crack growth in low alloying artificially aged 2xxx aluminium alloys. *Int. J. Fatigue*, 2007, 29: 869-878.
- [79] Cvijović Z, Cvijović I, Vratnica M. Fracture micromechanisms in overaged 7000 alloy forgings. *J. Alloys Compds.*, 2007, 441(1): 66-75.
- [80] Desmukh M N, Pandey R K, Mukhopadhyay A K. Effect of aging treatments on the kinetics of fatigue crack growth in 7010 aluminum alloy. *Mater. Sci. Eng. A*, 2006, 435: 318-326.
- [81] Burns J T, Boselli J. Effect of plate thickness on the environmental fatigue crack growth behavior of AA7085-T7451. *Int. J. Fatigue*, 2016, 83: 253-268.
- [82] Kawabata T, Izumi O. Ductile fracture in the interior of precipitate free zone in an Al-6.0%Zn-2.6%Mg

- alloy. *Acta Metall.*, 1976, 24: 817-825.
- [83] Hornbogen E, Gahr K H Z. Microstructure and fatigue crack growth in γ -Fe-Ni-Al alloy. *Acta Metall.*, 1976, 24(6): 581-592.
- [84] Zhang Y H, Edwards L. On the blocking effect of grain boundaries on small crystallographic fatigue crack growth. *Mater. Sci. Eng. A*, 1994, 188 (1-2): 121-132.
- [85] Morris W L. The noncontinuum crack tip deformation behavior of surface microcracks. *Metall. Mater. Trans. A*, 1980, 11 (7): 1117-1123.
- [86] Tanaka K, Akiniwa Y, Nakai Y, et al. Modelling of small fatigue crack growth interacting with grain boundary. *Eng. Frac. Mech.*, 1986, 24 (6): 803-819.
- [87] Sanders R E, Starke E A. The effect of intermediate thermomechanical treatments on the fatigue properties of a 7050 aluminum alloy. *Metall. Trans. A*, 1978, 9 (8): 1087-1100.
- [88] Sangid M D, Ezaz T, Sehitoglu H, et al. Energy of slip transmission and nucleation at grain boundaries. *Acta Mater.*, 2011, 59: 283-296.
- [89] De P S, Mishra R S, Smith C B. Effect of microstructure on fatigue life and fracture morphology in an aluminum alloy. *Scripta Mater.*, 2009, 60: 500-503.
- [90] Shao C W, Zhang P, Zhu Y K, et al. Improvement of low-cycle fatigue resistance in TWIP steel by regulating the grain size and distribution. *Acta Mater.*, 2017, 134: 128-142.
- [91] Liu G, Winwood S, Rhodes K, et al. The effects of grain size, dendritic structure and crystallographic orientation on fatigue crack propagation in IN713C Nickel-based superalloy. *Int. J. Plasticity*, 2020, 125: 150-168.
- [92] Lee W J, Chia W J, Wang J L, et al. Role of surfaces and interfaces in controlling the mechanical properties of metallic alloys. *Langmuir*, 2010, 26 (21), 16254-16260.
- [93] Starke E A, Staley J T. Application of modern aluminum alloys to aircraft. *Prog. Aero. Sci.*, 1996, 32 (2): 131-172.
- [94] Yates J R, Shi G, Atkinson H V, et al. Fatigue tolerant design of steel components based on the size of large inclusions. *Fatigue Fract. Eng. Mater. Struct.*, 2002, 25: 667-676.
- [95] Marquis F D S. Microstructural design of 7X50 aluminum alloys for fracture and fatigue. *Nano and Microstructural Design of Advanced Materials*, Ed., M. A. Mayers, R. O. Ritchie, M. Sarikaya. Elsevier, 2003, p. 271-286.
- [96] Shikama T, Yoshihara S. Highly SCC resistant 7000-series aluminum alloy extrusion. *KOBELCO Tech. Rev.*, 2017, 35: 65-68.
- [97] Ogura T, Sato T. Controlled nano-clusters in the vicinity of grain boundaries and improved strength and ductility of Al-Zn-Mg based alloys. *J. Japan Inst. Light Metals*, 2013, 63 (5): 196-203.
- [98] Lin L, Liu Z, Liu W, et al. Effects of Ag addition on precipitation and fatigue crack propagation behavior of a medium-strength Al-Zn-Mg alloy. *J. Mater. Sci. Tech.*, 2018, 34 (3): 534-540.